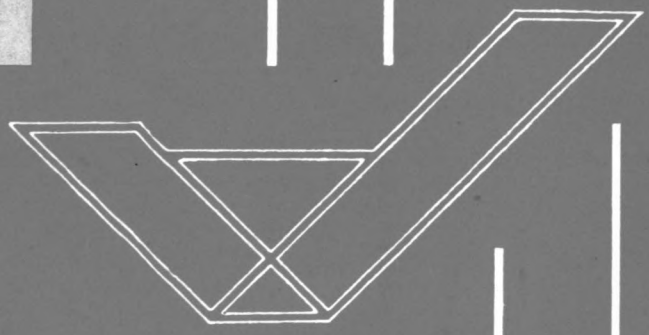
VM-GLF- 3048
Mossel- 1985



report no. R/1985/H/1

Response of Wave Directions to Changes in Wind Direction

E. Mosselman

Delft University of Technology
Dep. of Civil Engineering
Fluid Mechanics Group

Response of Wave Directions to Changes in Wind Direction

by Erik Mosselman

January 1995

Delft University of Technology
Department of Civil Engineering

Foreword

This report describes an investigation of the directional response of sea waves to a changing wind direction. It has been written as a thesis at the Delft University of Technology.
The results have also been presented at the Symposium on Description and Modelling of Directional Seas, held in June 1984 in Copenhagen, Denmark (14).

Mentors:

prof. dr. ir. J. A. Battjes

dr. ir. L. H. Holthuijsen

Summary

A relaxation model for the response of the main wave direction to changes in wind direction is derived with a parametric approach of the energy balance of locally generated waves. An expression to quantify the time scale of this model is obtained from empirical growth relations of waves in a fetch-unlimited situation. The model is compared with observations in the southern North Sea with a pitch-and-roll buoy. The model seems to be consistent with the observations.

Table of Contents

	page
1. Introduction	1
2. The Model	
2.1 Derivation	3
2.2 Substitution of Empirical Wave Growth Relations	6
3. Observations	
3.1 Measurement Sites and Periods	10
3.2 Data Acquisition	11
3.3 Data Selection	12
4. Analysis and Results	14
5. Discussion and Conclusions	
5.1 Discussion	15
5.2 Conclusions	17
Acknowledgments	18
References	19
Appendices	
A: Empirical wave growth relations	22
B: Determination of the main wave direction	24
C: Relaxation models proposed in the literature	26
D: Directional response in Klatter's ECG model	28
E: Correction for the difference angle	29

1. Introduction

Shipping, offshore mining and protection of coastal areas require knowledge of sea waves. In this field wave directionality has become an important topic. An interesting question is how wave directions respond to changes in wind direction, especially since the SWAMP study (23) revealed that present wave prediction models diverge with regard to directional response.

Generally the local wind tends to align the waves into the local wind direction. In the case of a turning wind the wave directions turn as well in order to reach a new equilibrium state. The wind provides the energy for this process, so the stronger the wind, the faster the waves respond. Since high frequencies grow faster than lower frequencies, they also respond faster to a change in wind direction.

Kuik and Holthuijsen (19) describe that a qualitative difference exists between the response to slowly turning winds and that to rapidly turning winds. When the wind turns slowly the energy density spectrum remains unimodal, i.e. single-peaked. The mean wave direction lags behind the shifting wind direction, with the lag decreasing as the frequency increases. When the wind turns rapidly new waves are generated at the high frequencies with a mean direction approximately equal to the new wind direction, thus yielding a bimodal, i.e. double-peaked energy density spectrum. Such sudden changes of wind direction are mostly caused by frontal passages. A part of the wind sea becomes swell and may disappear by radiation from the considered area.

Still many other factors influence wave directions. Turning winds are usually associated with a nonhomogeneous windfield, so that elsewhere waves may be generated and radiated into the considered area in a direction entirely deviating from that of the local wind. Currents and bottom bathymetry may influence wave directions by means of refraction. High frequencies are more sensitive to currents because of their lower celerities, while low frequencies are more sensitive to water depth because of their larger wave-lengths. The coast-line geometry can also have a strong influence on wave directions. For instance, it has been observed that slanting offshore winds caused waves to travel almost parallel to the coast-line.

Some simple relaxation models to describe the directional response are proposed in the literature, assuming spatial homogeneity and no influences from currents, shoals or coasts. Günther, Rosenthal and Dunckel (8) give a relaxation model for the direction of the total momentum flux, while Hasselmann, Dunckel and Ewing (9) present a frequency dependent relaxation model for mean directions.

In the present research the problem is approached both theoreticly and experimentally. A directional relaxation model is derived by a parametric approach of the spectral energy balance equation. This results in an expression for the response of the mean direction of the full frequency range, with a nondimensional time scale depending on the stage of development of the wavefield. The relation between this time scale and the stage of development can be quantified by substituting empirical wave growth relations. This implies that differences between various wave growth relations cause variations in model predictions of time scales.

To compare the model with observations, measurements have been carried out with a pitch-and-roll buoy in the southern North Sea: Unfortunately currents, bottom bathymetry and coast-line geometry did play a role at the measurement sites. Though observed time scales agreed qualitatively with the model they still scattered considerably, in spite of a rather strict selection of the observations. This may be partly due to the site limitations and the inherent errors in the observations. Furthermore, less scatter can hardly be expected in view of the uncertainties in empirical wave growth parameters.

The model appears to be close to that of Günther et al., but rather different from that of Hasselmann et al. The model also supports the directional response of waves in the numerical wave prediction model developed by Klatter (10).

2. The Model

2.1 Derivation

Nonlinear wave-wave interactions have a stabilizing effect on the shape of young sea spectra. This provides a possibility to derive parametric expressions for sea spectrum growth from the energy balance equation (10). The derivation of the present directional relaxation model is essentially the same. It consists of applying the operator which defines the main wave direction in terms of the wave spectrum to the energy balance equation. The operator has been chosen in accordance with the usual analysis of pitch-and-roll buoy data (see Appendix B)

$$\theta_o = \arctan\left(\frac{b_1}{a_1}\right) \qquad (2-1)$$

in which

$$a_1 = \frac{\int_0^{2\pi}\int_0^{\infty} \cos\theta \; E(f,\theta)\, df\, d\theta}{\int_0^{2\pi}\int_0^{\infty} E(f,\theta)\, df\, d\theta} \qquad (2-2)$$

$$b_1 = \frac{\int_0^{2\pi}\int_0^{\infty} \sin\theta \; E(f,\theta)\, df\, d\theta}{\int_0^{2\pi}\int_0^{\infty} E(f,\theta)\, df\, d\theta} \qquad (2-3)$$

and $E(f,\theta)$ is the energy density at the wave component with frequency f coming from direction θ.

The spectral energy balance can be written as

$$\frac{\partial E(f,\theta)}{\partial t} + \nabla c_g(f,\theta)\, E(f,\theta) = S(f,\theta) \qquad (2-4)$$

in which c_g is the energy transport velocity and $S(f,\theta)$ is the source function representing wave growth and decay mechanisms. In a homogeneous wavefield this reduces to

$$\frac{\partial E(f,\theta)}{\partial t} = S(f,\theta) \qquad (2-5)$$

Defining the main direction of the source function, θ_s, analogously to the main wave direction gives

$$\theta_s = \arctan\left(\frac{\beta_1}{\alpha_1}\right) \tag{2-6}$$

with

$$\alpha_1 = \frac{\int_0^{2\pi}\int_0^{\infty} \cos\theta \; S(f,\theta)\, df\, d\theta}{\int_0^{2\pi}\int_0^{\infty} S(f,\theta)\, df\, d\theta} \tag{2-7}$$

$$\beta_1 = \frac{\int_0^{2\pi}\int_0^{\infty} \sin\theta \; S(f,\theta)\, df\, d\theta}{\int_0^{2\pi}\int_0^{\infty} S(f,\theta)\, df\, d\theta} \tag{2-8}$$

Elaboration of the above equations yields

$$\frac{\partial \theta_o}{\partial t} = \frac{\cos\theta_o}{\cos\theta_s} \frac{\int_0^{2\pi}\int_0^{\infty} S(f,\theta)\cos\theta \; df\, d\theta}{\int_0^{2\pi}\int_0^{\infty} E(f,\theta)\cos\theta \; df\, d\theta} \sin(\theta_s - \theta_o) \tag{2-9}$$

Assuming that the shape of the directional distribution of $S(f,\theta)$ is equal to that of $E(f,\theta)$ and writing the integrations of $E(f,\theta)$ and $S(f,\theta)$ over directions as $E(f)$ and $S(f)$ respectively, the rate of change of θ_o can be written as

$$\frac{\partial \theta_o}{\partial t} = \frac{\int_0^{\infty} S(f)\, df}{\int_0^{\infty} E(f)\, df} \sin(\theta_s - \theta_o) \tag{2-10}$$

Furthermore it is assumed that the wind direction is equal to the main direction of the source function

$$\theta_w = \theta_s \tag{2-11}$$

A nondimensional wave energy, $\tilde{E}$, and a nondimensional time, $\tilde{t}$, can be defined by using the wind speed, U, and the acceleration due to gravity, g:

$$\tilde{\varepsilon} = \frac{g^2}{U^4} \int_0^\infty E(f)\, df \qquad (2\text{-}12)$$

and

$$\tilde{t} = \frac{g\, t}{U} \qquad (2\text{-}13)$$

Then Equation (2-10) can be written as

$$\frac{\partial \theta_o}{\partial \tilde{t}} = \frac{1}{\tilde{\varepsilon}} \frac{\partial \tilde{\varepsilon}}{\partial \tilde{t}} \sin(\theta_w - \theta_o) \qquad (2\text{-}14)$$

or

$$\frac{\partial \theta_o}{\partial \tilde{t}} = \frac{1}{\tilde{\tau}} \sin(\theta_w - \theta_o) \qquad (2\text{-}15)$$

in which

$$\tilde{\tau} = \left(\frac{1}{\tilde{\varepsilon}} \frac{\partial \tilde{\varepsilon}}{\partial \tilde{t}} \right)^{-1} \qquad (2\text{-}16)$$

This relaxation model is elaborated in the following sections.

2.2 Substitution of Empirical Wave Growth Relations

The growth of wave energy in deep water as a function of time in a fetch-unlimited, homogeneous windfield can be approximated by

$$\tilde{\varepsilon} = a \tanh^{d}(b \tilde{t}^{c}) \qquad (2-17)$$

for cases in which the wave direction equals the wind direction. Many numerical wave prediction models are based on such an expression, each with its own parameter values. They can be substituted in Equation (2-16). The effect of differences in parameter values is shown in Figure 2.1 by using three models considered in the SWAMP study (23): SAIL, BMO and GONO. Appendix A gives more details of the computation.

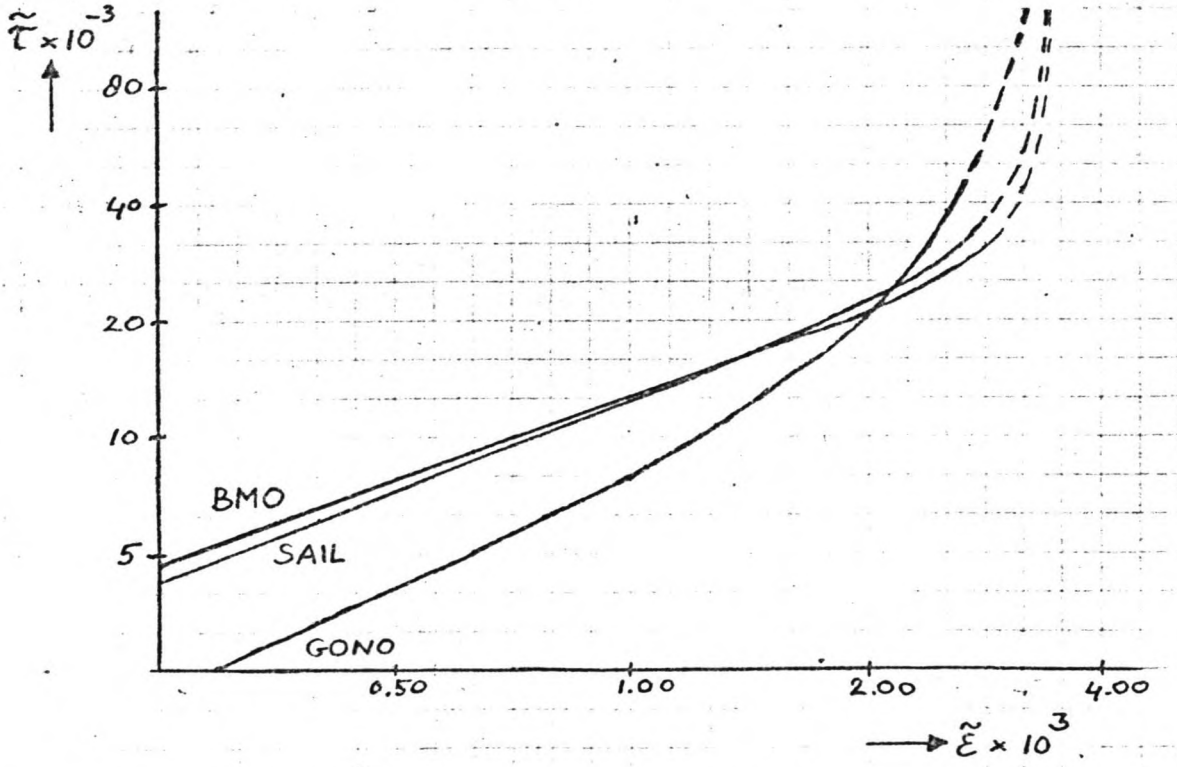


Fig. 2.1 Plot of $\tilde{\tau}$ vs. $\tilde{\varepsilon}$ derived from the substitution of different wave growth relations.

The parts of the curve corresponding to a fully developed sea state are indicated by dashed lines, since the derived model only holds for young sea states.

The complete family of wave growth curves in the SWAMP study can be characterized by an upper and a lower limit, see Appendix A. The relation between $\tilde{\tau}$ and $\tilde{\varepsilon}$ can be represented then by the shaded area in Figure 2.2.

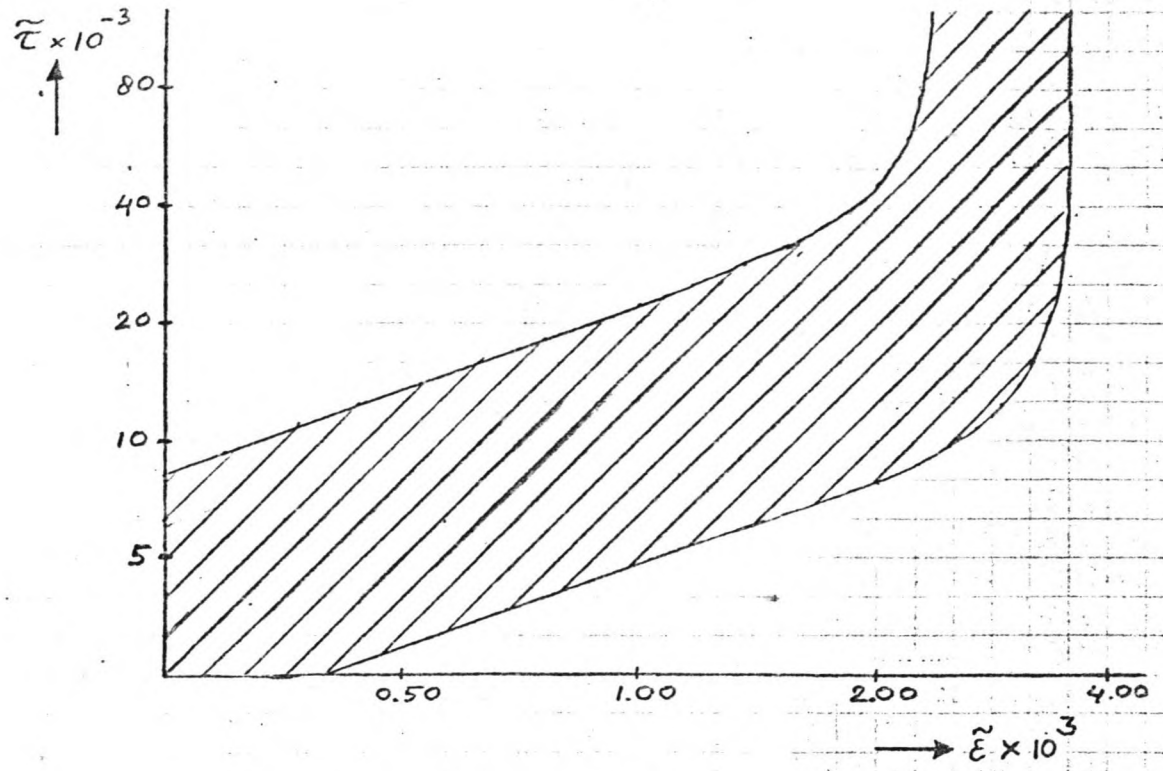


Fig. 2.2 Plot of $\tilde{\tau}$ vs. $\tilde{\varepsilon}$ derived from an upper and a lower limit to wave growth curves presented in the SWAMP study.

The model can easily be extended to shallow water by forcing $\tilde{\varepsilon}$ to a lower limit for $\tilde{\tau} \to \infty$ by replacing a and b in Equation (2-17)

$$a \longrightarrow a \tanh^2 (\beta \tilde{d}^{\gamma}) \qquad (2\text{-}18)$$

$$b \longrightarrow b / \tanh^{2/d} (\beta \tilde{d}^{\gamma}) \qquad (2\text{-}19)$$

where $\tilde{d}$ is the nondimensional water depth given by

$$\tilde{d} = \frac{g d}{U^2} \qquad (2\text{-}20)$$

From Groen and Dorrestein (7) Holthuijsen (12) finds

$$\beta = 0.71 \qquad (2\text{-}21)$$

$$\gamma = 0.76 \qquad (2\text{-}22)$$

The corresponding dependency of $\tilde{\tau}$ on $\tilde{\varepsilon}$ is given in Figure 2.3 .

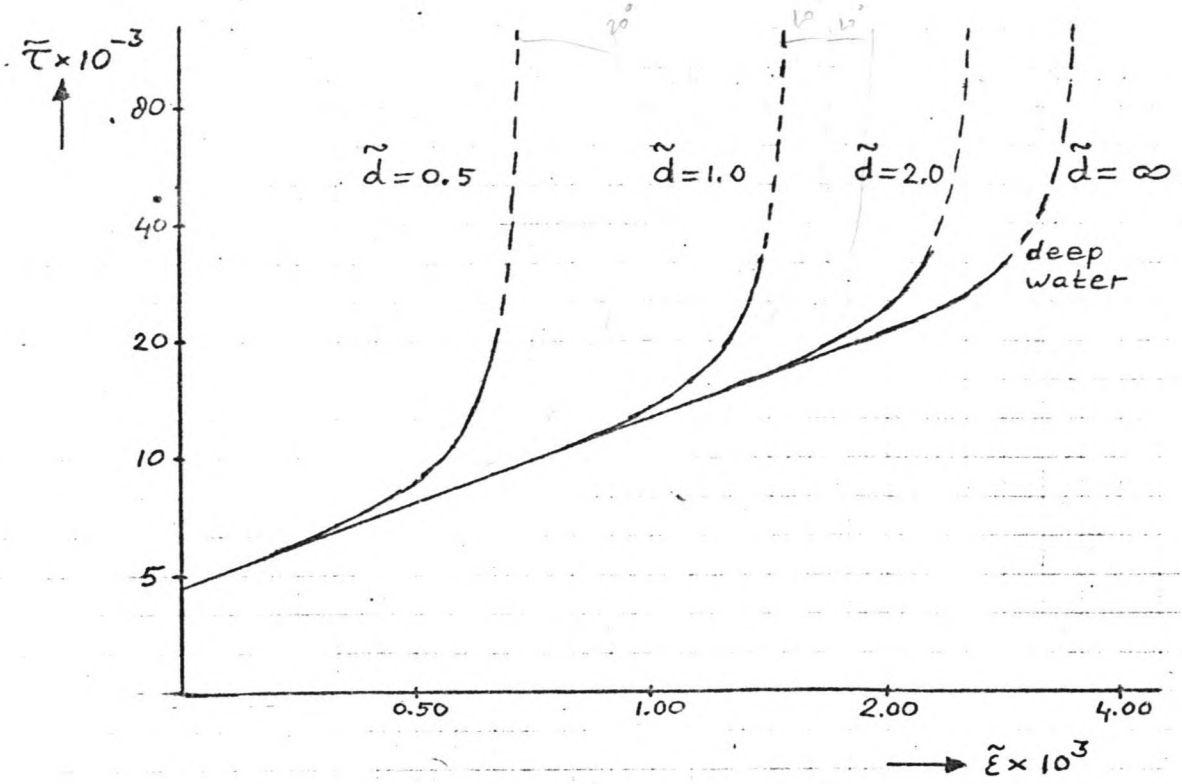


Fig. 2.3 Plot of $\tilde{\tau}$ vs. $\tilde{\varepsilon}$ based on the BMO model with the nondimensional depth $\tilde{d}$ as a parameter.

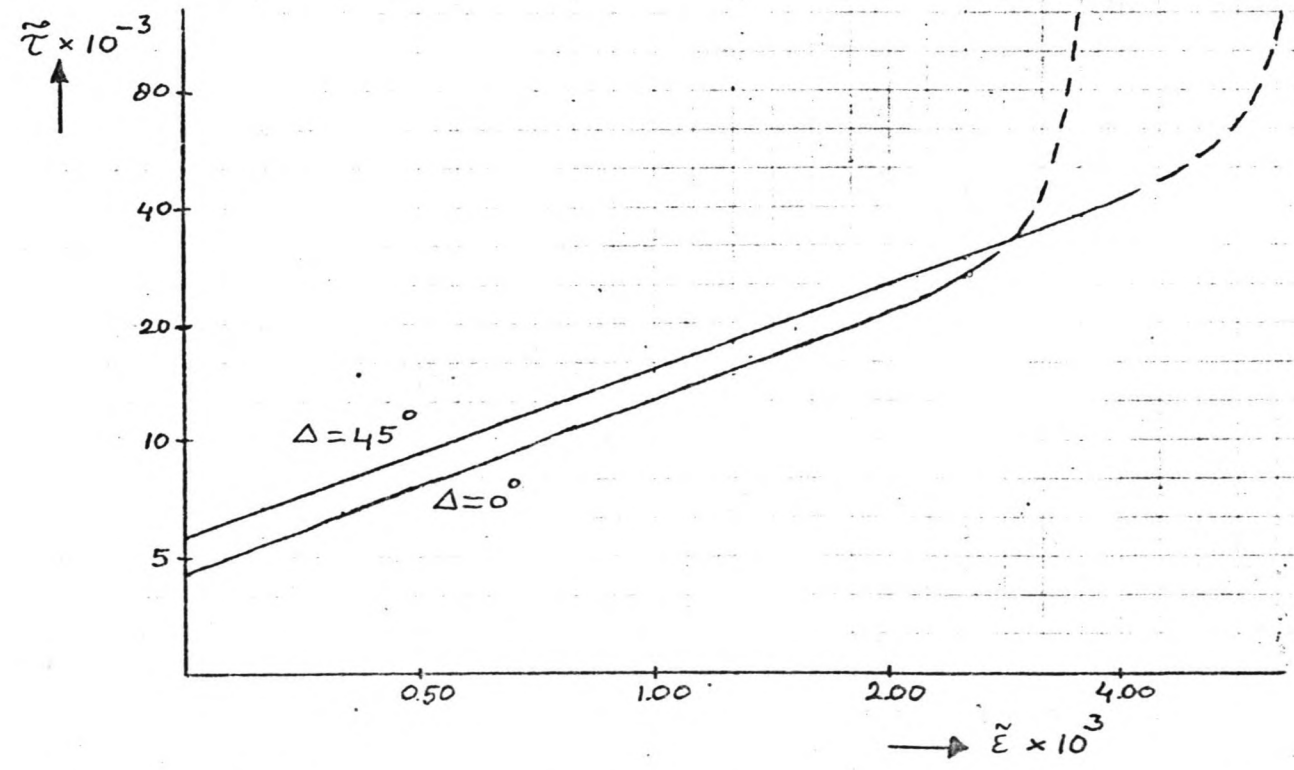


Fig. 2.4 Plot of $\tilde{\tau}$ vs. $\tilde{\varepsilon}$ based on the BMO model with a correction for the difference angle Δ.

The empirical wave growth relations are determined for a homogeneous windfield and a constant wind direction, so actually Equation (2-17) only holds for $\theta_o = \theta_w$. After a change in wind direction only a part of the extant wave energy will contribute to the new wind sea ; waves will grow as though the actual wave energy is lower.
Holthuijsen (personal communication) proposes to incorporate this in the model by taking the derivative of $\tilde{\varepsilon}$ in Equation (2-16) at a lower energy level, $\tilde{\varepsilon}^*$, depending on $\tilde{\varepsilon}$ and the absolute value of the difference angle, Δ, given by

$$\Delta = |\theta_w - \theta_o| \qquad (2\text{-}23)$$

More details are given in Appendix E.
The effect on $\tilde{\tau}$ is given in Figure 2.4 for $\Delta = 45°$.

3. Observations

3.1 Measurement Sites and Periods

In 1982 measurements were carried out at locations near the Dutch coast in the southern North Sea, see Figure 3.1. At these sites waves were influenced by bottom bathymetry and coast-line geometry. Furthermore tidal currents occurred up to 1.5 m/s.

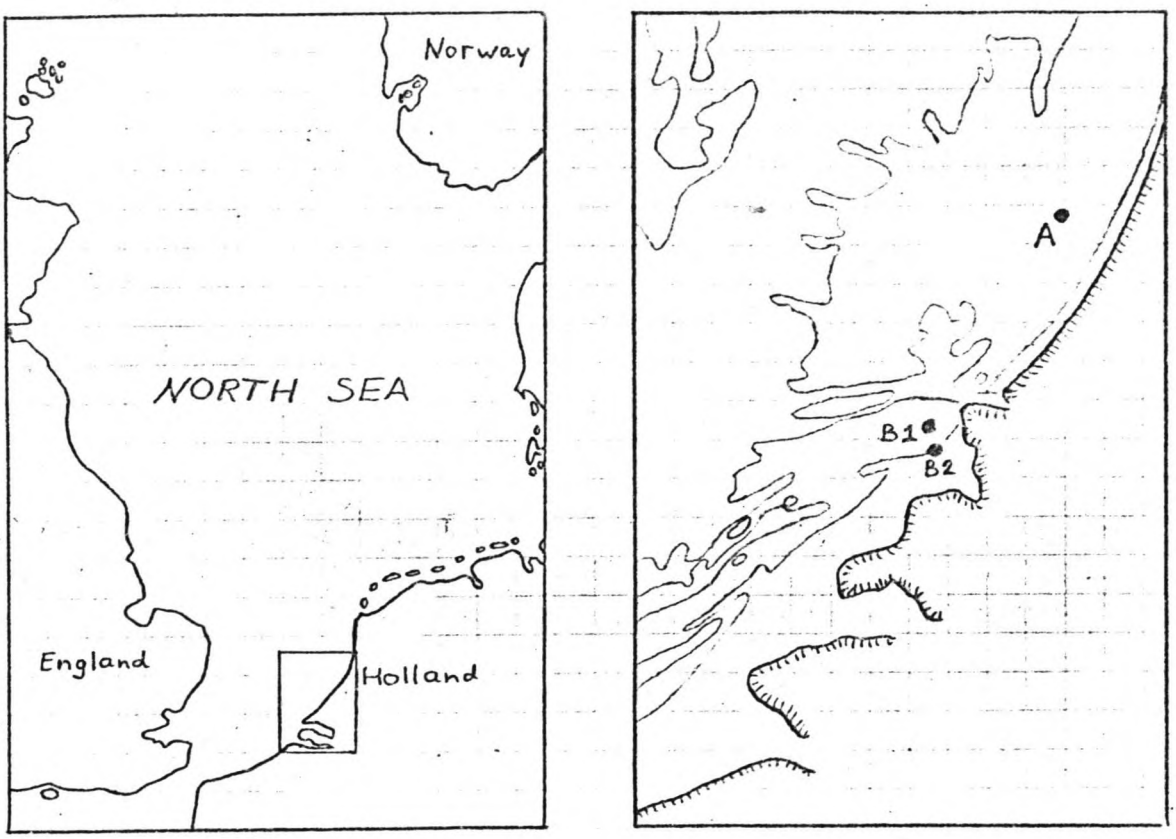


Fig. 3.1 Measurement sites A and B

Observations were performed during two periods, one at site A and one at site B. This is emphasized here because the manner of data acquisition and analysis is slightly different for each of these periods.

Site A represents a location near the research tower "Meetpost Noordwijk". Site B actually consists of two locations, both in the Haringvliet mouth. Some data are listed below.

Table 3.1 Measurement sites and periods

period	site	mean water depth
9 – 15 March 1982	A	17 m
10 Sept. – 29 Oct. 1982	B, location 1	15.3 m
29 Oct. – 5 Nov. 1982	B, location 2	10.6 m

3.2 Data Acquisition

Wave parameters were obtained by using Datawell's WAVEC pitch-and-roll buoy, which is described by Van der Vlugt, Kuik and Holthuÿsen (24). The elevation and slope signals were spectrally analyzed thus yielding the frequency spectrum, $E(f)$, and the first four Fourier coefficients of the directional spreading function, $D_f(\theta)$, with frequency steps of 0.005 Hz. From these data several wave parameters were determined. The wave parameters were mostly given at 60 minutes intervals, but at site A also 30 and 120 minutes intervals have been used.

For each location wind speed and wind direction were measured at a nearby observation tower with a cup anemometer and a vane.
At site A 10 minutes averages were obtained each 30 minutes at an elevation of 27.4 m above mean sea level.
The averaging process was carried out vectorially, which implies that directions were weighted with velocities.
By using the results of a scale model study performed by the National Aerospace Laboratory of the Netherlands (22) the data have been corrected for the influence of the observation tower. After that the wind velocities have been converted to an elevation of 10 m above mean sea level by assuming a logarithmic velocity profile with drag coefficient $C_{D10} = 1.5 \times 10^{-3}$.
At site B the wind data were obtained at 13 m above mean sea level. They were treated in a somewhat less accurate way. Each hour wind data were given. The wind speed was the average of the last ten minutes, but the wind direction was the average of only two wind vane observations: one at five minutes to the full hour and one at the full hour itself.
The Delta Department of the Dutch Ministry of Transport and Public Works suspects a systematic wind direction error of three degrees, but its effect cannot be recovered afterwards since wind directions were rounded to the nearest multiple of ten degrees. These uncertainties in wind direction may contribute substantially to the overall error. Suppose as an extreme example that the wind direction deviated 12° from the main wave direction at a certain moment at site B. Because of the suspected systematic error of 3° this would have been recorded as 15°, becoming 20° after the rounding-off. This would imply an error of 67 % in the difference angle, $\theta_w - \theta_o$.
Again the wind velocities have been converted to an elevation of 10 m above mean sea level by assuming a logarithmic velocity profile with $C_{D10} = 1.5 \times 10^{-3}$, but no correction has been made for the influence of the (slender) tower.

3.3 Data Selection

In order to distil useful information from the data various selection criteria have been applied. These will be explained below.

When the wave direction equals the wind direction no directional response occurs. But for small deviations it is also hard to discern any response, because the information gets lost on account of directional resolution limitations. Besides, the less the directions deviate the more the results will be influenced by the uncertainties in the observed wind directions at site B, which are caused by the rounding-off to multiples of ten degrees. These considerations have led to a lower limit of the difference angle

$$|\theta_w - \theta_o| \geq 10^\circ \qquad (3-1)$$

Since testing a relaxation model was the purpose of the investigation, only cases with a wave direction turning towards the wind direction have been taken into account. This has been expressed as follows:

$$\theta_o > \theta_w \quad \text{if} \quad \theta_o \text{ decreases} \qquad (3-2)$$

and

$$\theta_o < \theta_w \quad \text{if} \quad \theta_o \text{ increases} \qquad (3-3)$$

In the model the waves are assumed to be growing under the local wind. Therefore the observations should not be contaminated by swell. Elimination of swell cases also implies that only gradually varying wind directions are taken into account, since rapidly turning winds cause bimodal spectra containing swell.
Swell can be distinguished from the wind sea by considering the Pierson-Moskowitz frequency

$$f_{PM} = 0.13 \frac{g}{U} \qquad (3-4)$$

Frequencies below the Pierson-Moskowitz frequency represent swell.

Three simultaneously applied swell criteria have been formulated

1. The wave energy at frequencies below the Pierson-Moskowitz frequency should be less than five percent of the total wave energy

$$\int_0^{f_{PM}} E(f)\,df < 0.05 \int_0^{\infty} E(f)\,df \qquad (3-5)$$

2. The peak frequency should be higher than the Pierson-Moskowitz frequency, here defined with the wind speed component in the main wave direction

$$f_m > 0.13 \frac{g}{U \cos(\theta_w - \theta_0)} \qquad (3-6)$$

3. Only difference angles less than ninety degrees should be taken into account

$$|\theta_w - \theta_0| < 90^\circ \qquad (3-7)$$

To eliminate coastal influences only on-shore wind conditions have been accepted.
For the observations to be accepted, the angle between the wind direction and the coast-line should be at least thirty degrees (arbitrarily chosen value), see Figure 3.2.
Note that directions indicate where the wind and waves are coming from.

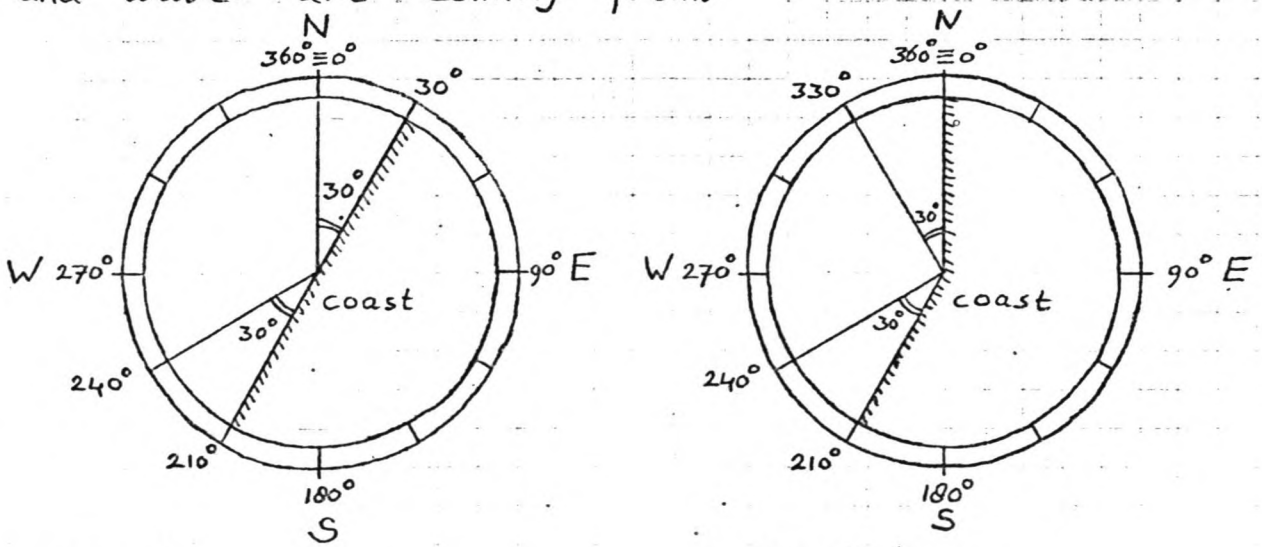


Fig. 3.2 Choice of wind direction sectors

4. Analysis and Results

From about 1400 records (each containing wind and wave parameters of a specific point of time) only 8 records survived the selection. From the selected data values of the nondimensional time scale, $\tilde{\tau}$, have been determined with a reciprocal form of Equation (2-15)

$$\tilde{\tau}_i = \frac{2\,\Delta t}{\theta_{0,i+1} - \theta_{0,i-1}} \frac{g}{U_i} \sin\left(\theta_{w,i} - \theta_{0,i}\right) \qquad (4-1)$$

where Δt denotes the interval between successive points of time and i denotes the rank number of these points of time.
The results are shown in Figure 4.1.

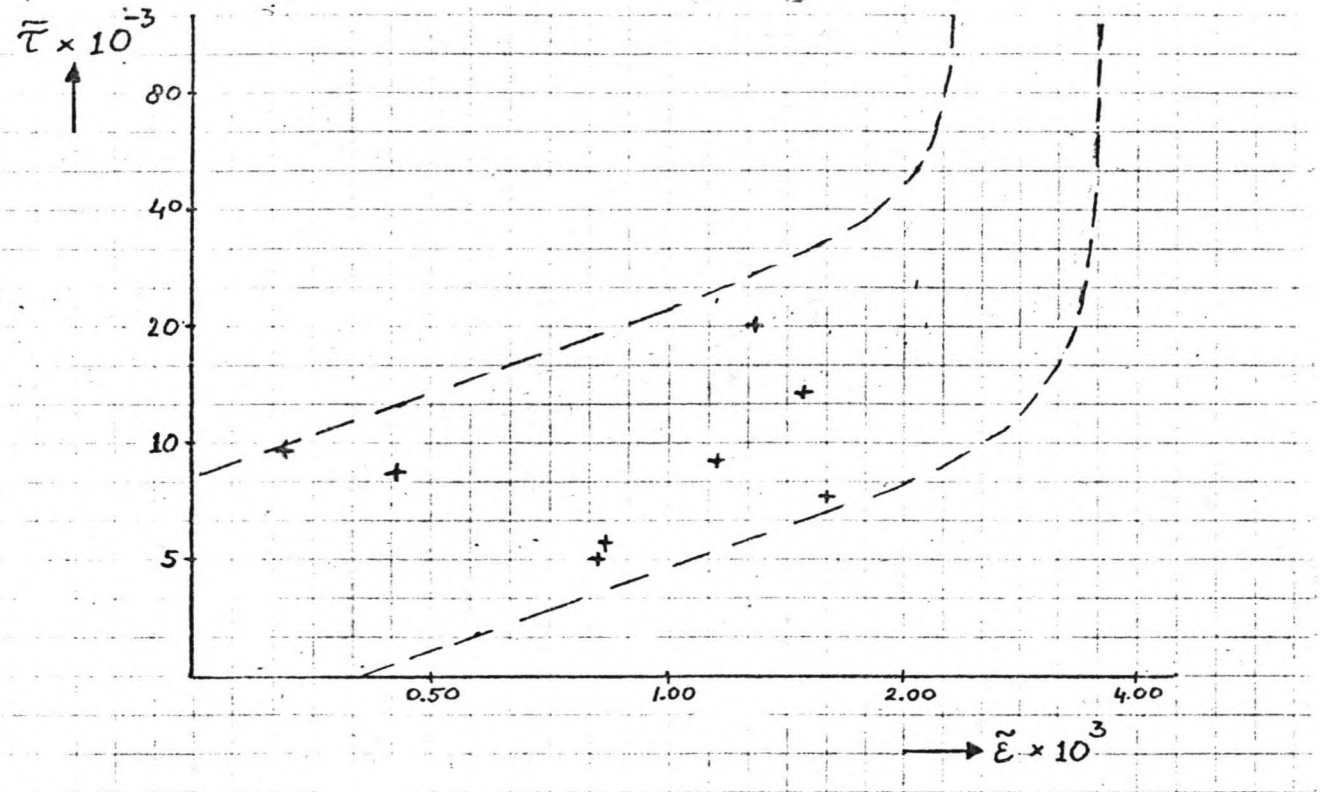


Fig. 4.1 Plot of $\tilde{\tau}$ vs. $\tilde{\varepsilon}$ from the observations. The dashed lines indicate the upper and lower limits as given in Figure 2.2.

For these selected observations wind velocities ranged between 10 and 20 m/s. Current velocities ranged up to 1.1 m/s. None of the selected observations was obtained at location B2.

5. Discussion and Conclusions

5.1 Discussion

The observations scatter considerably, but they are consistent with the model. In spite of this consistency, the scatter may be largely due to the inherent errors in the observations. Especially the uncertainties in wind direction data obtained at site B may have contributed substantially to these errors. Furthermore, the geophysical conditions were far from ideal (shallow water, currents, coastal influences).

A very striking result is that from a large number of observations only a few data remained on account of a rather strict selection. Much more measurements are needed for a better verification of the model, preferably carried out in better geophysical conditions. Fortunately, such measurements can be expected in the near future.

The measurements were carried out in shoaling water conditions. The shallow water extension of the model is not simply applicable here, because it has been derived for a constant water depth. Besides, the shallow water influence on the model is reduced by the correction for the difference angle, Δ.

A comparison with two directional relaxation models from the literature is shown in Figure 5.1. More detailed information can be found in Appendix C. The model of Günther et al. (8) agrees well with the present study, but the model for peak frequency of Hasselmann et al. (9) is remarkably different. The mean direction at the peak frequency responds in the model of Hasselmann et al. much slower than that of the full frequency range.

Klatter (10) investigated the directional response behaviour of his ECG wave prediction model under a stationarily turning wind. Figure 5.2 shows that his results agree with the present study. More information can be found in Appendix D.

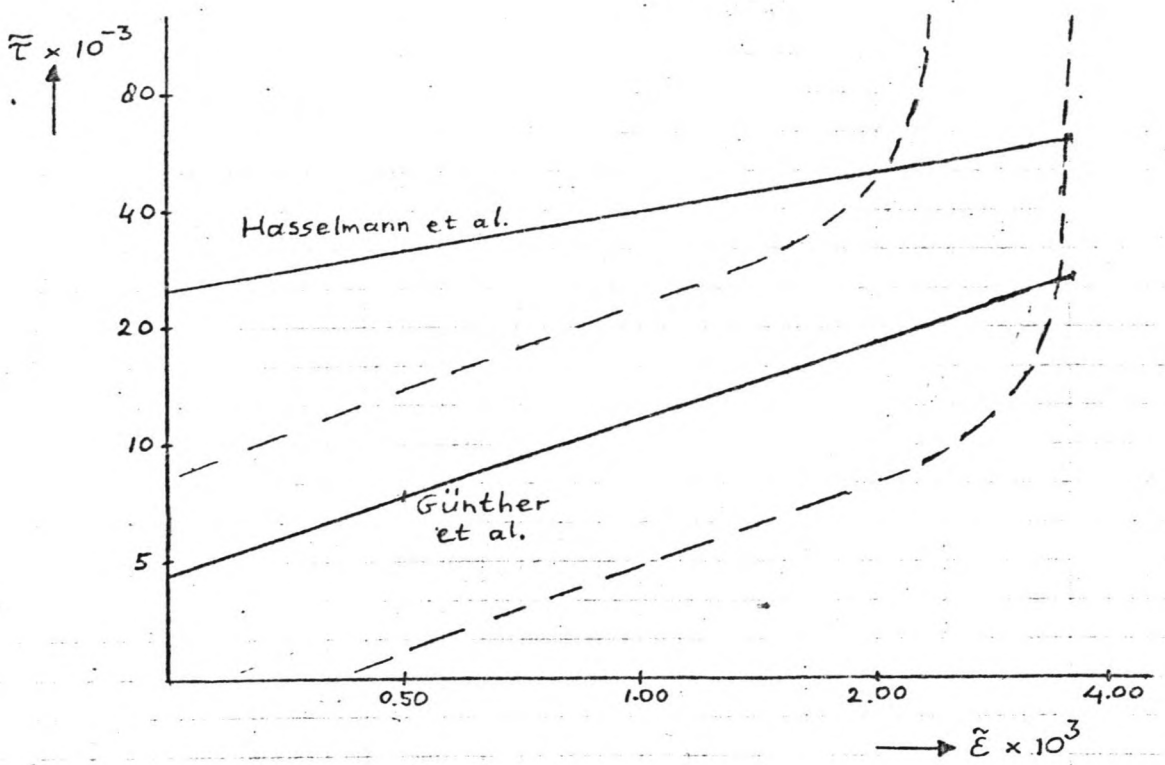


Fig. 5.1 Plot of $\tilde{\tau}$ vs. $\tilde{\varepsilon}$ from the models of Günther et al. and Hasselmann et al. The dashed lines indicate the upper and lower limits as given in Figure 2.2.

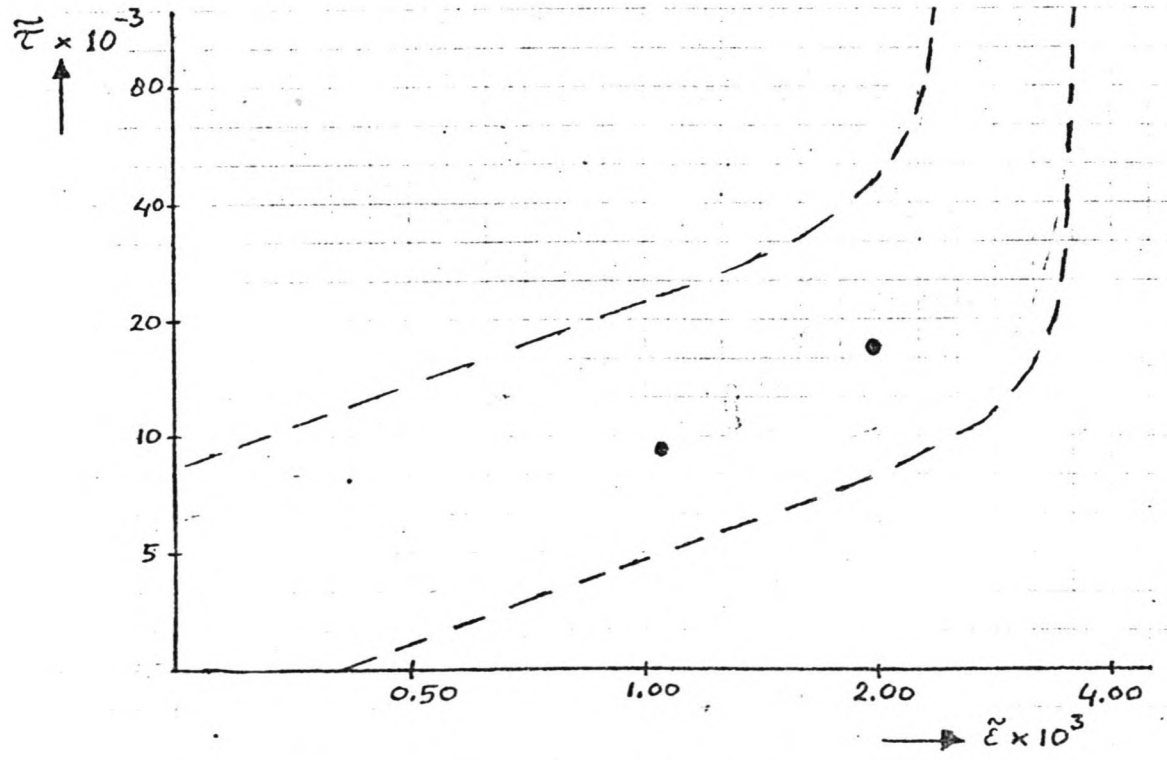


Fig. 5.2 Plot of $\tilde{\tau}$ vs. $\tilde{\varepsilon}$ from Klatter's ECG model. The dashed lines indicate the upper and lower limits as given in Figure 2.2.

5.2 Conclusions

- A simple model for the response of the main wave direction to changes in wind direction can be derived from the energy balance of the waves. Only empirical information on wave growth is used, no empirical information on wave directionality.

- Observations agree qualitatively well with the model. However, from a large number of observations only a few remained after a rather strict selection. More measurements are needed for a better verification of the model. These measurements should be carried out in deep water conditions without coastal influences.

- The model agrees with the directional relaxation model of Günther et al., but is rather different from that of Hasselmann et al.

- The present study agrees with the directional response predictions of Klatter's ECG model.

Acknowledgments

I gratefully acknowledge the opportunity to use data and equipment of the Ministry of Transport and Public Works of the Netherlands.
Among its employees, thanks are especially due to

ir. A.J. Kuik	for providing data and for valuable discussions
ir. A.J.M. van der Vlugt	for providing data
J. Hoekema	for assistance with computer work

References

1. Allender, J.H., J. Albrecht and G. Hamilton, 1983
Observations of directional relaxation of wind sea spectra
Journal of Physical Oceanography, Vol. 13, pp. 1519-1525

2. Battjes, J.A.
Lecture notes b78 Windgolven
Technische Hogeschool Delft, Afdeling der Civiele Techniek

3. Bendat, J.S. and A.G. Piersol, 1971
Random data: analysis and measurement procedures
Wiley-Interscience

4. Borgman, L.E.
Directional wave spectra from wave sensors
Marine Science, Vol. 8: Ocean Wave Climate
Edited by M.D. Earle and A. Malahoff
National Oceanic and Atmospheric Administration

5. CERC, 1973
Shore Protection Manual
U.S. Army Coastal Engineering Research Center, Corps of Engineers

6. Deltadienst, 1980
Golfverwachtingen op de Noordzee en aan de Nederlandse kust
Driemaandelijks Bericht Deltawerken
Deltadienst, 's Gravenhage

7. Groen, P. and R. Dorrestein, 1976
Zeegolven, Opstellen op oceanografisch en maritiem meteorologisch gebied, no. 11
's Gravenhage

8. Günther, H., W. Rosenthal and M. Dunckel, 1981
The response of surface gravity waves to changing wind direction
Journal of Physical Oceanography, Vol. 11, pp. 718-728

9. Hasselmann, D.E., M. Dunckel and J.A. Ewing, 1980
Directional wave spectra observed during JONSWAP 1973
Journal of Physical Oceanography, Vol. 10, pp. 1264-1280

10. Hasselmann, K., T.P. Barnett, E. Bouws, H. Carlson, D.E. Cartwright, K. Enke, J.A. Ewing, H. Gienapp, D.E. Hasselmann, P. Kruseman, A. Meerburg, P. Müller, D.J. Olbers, K. Richter, W. Sell and H. Walden, 1973
Measurements of wind-wave growth and swell decay during the Joint North Sea Wave Project (JONSWAP)
Ergänzungsheft zur Deutschen Hydrographischen Zeitschrift, Reihe A(8), No. 12, 1973

11. Hasselmann, K., D.B. Ross, P. Müller and W. Sell, 1976
A parametric wave prediction model
Journal of Physical Oceanography, Vol. 6, pp. 200-228

12. Holthuijsen, L.H., 1979
Methoden voor golfvoorspelling
Technische Adviescommissie voor de Waterkeringen
's Gravenhage, 1980

13. Holthuijsen, L.H., 1981
Wave directionality as inferred from stereo photos
Proceedings of the Conference on Directional Wave
Spectra Applications, 14-16 September 1981,
University of California, Berkeley, California
Edited by R.L. Wiegel

14. Holthuijsen, L.H., E. Mosselman and A.J. Kuik, 1984
A model for the response of wave directions to
changes in wind direction
Paper No. C-4 of the Symposium on Description and
Modelling of Directional Seas, 18-20 June 1984,
Technical University of Denmark, Copenhagen, Denmark

15. Janssen, P.A.E.M., G.J. Komen and W.J.P. de Voogt
GONO, a coupled hybrid wave prediction model
submitted for publication, May 1983

16. Jenkins, G.M. and D.G. Watts, 1968
Spectral analysis and its applications
Holden-Day

17. Kinsman, B., 1965
Wind Waves, Their generation and propagation on the ocean surface
Prentice-Hall

18. Klatter, H.E., 1983
Een tweeparameter golfvoorspellingsmodel
Technische Hogeschool Delft, Afdeling der Civiele Techniek
Vakgroep Vloeistofmechanica
R / 1983 / 5 / H

19. Kuik, A.J. and L.H. Holthuijsen, 1981
Buoy observation of directional wave parameters
Proceedings of the Conference on Directional Wave
Spectra Applications, 14-16 September 1981,
University of California, Berkeley, California
Edited by R.L. Wiegel

20. Kuik, A.J., 1981
Unpublished notes

21. Markus, J.C., 1982
Golfrichting, locale verwerkingseenheid in HP 9835, systeembeschrijving
Concept rapport aan de afdeling Hydro - Instrumentatie van Rijkswaterstaat

22. Maur, G. in der, 1976
Stromingsonderzoek in een windtunnel ten behoeve van de installatie van windmeetinstrumenten op de Meetpost Noordwijk
NLR TR 76140 L
National Aerospace Laboratory NLR, the Netherlands

23. SWAMP group, 1982
An intercomparison study of wind wave prediction models

24. Van der Vlugt, A.J.M., A.J. Kuik and L.H. Holthuijsen, 1981
The WAVEC directional buoy under development
Proceedings of the Conference on Directional Wave Spectra Applications, 14-16 September 1981, University of California, Berkeley, California
Edited by R.L. Wiegel

Appendix A: Empirical wave growth relations

The growth of wave energy as a function of time in a fetch-unlimited, homogeneous windfield can be approximated by

$$\tilde{\varepsilon} = a \tanh^{d}\left(b\,\tilde{t}^{\,c}\right) \qquad (A\text{-}1)$$

Hence

$$\frac{\partial \tilde{\varepsilon}}{\partial \tilde{t}} = a\,b\,c\,d\left(\frac{\tilde{\varepsilon}}{a}\right)^{\frac{d-1}{d}}\left[1-\left(\frac{\tilde{\varepsilon}}{a}\right)^{\frac{2}{d}}\right]\left[\frac{1}{b}\,\mathrm{arctanh}\left(\frac{\tilde{\varepsilon}}{a}\right)^{\frac{1}{d}}\right]^{\frac{c-1}{c}} \qquad (A\text{-}2)$$

Some numerical wave prediction models are based on such expressions. For the models SAIL, BMO and GONO, considered in the SWAMP study (23), the computed growth curves can be approximated with (A-1) and the parameter values as listed in Table A.1. A plot of $\tilde{\varepsilon}$ vs. $\tilde{t}$ for these models is given in Figure A.1.
The complete family of wave growth curves presented in de SWAMP study can be characterized by an upper and a lower limit based on the same expressions, see Figure A.2. The corresponding parameter values are also listed in Table A.1.

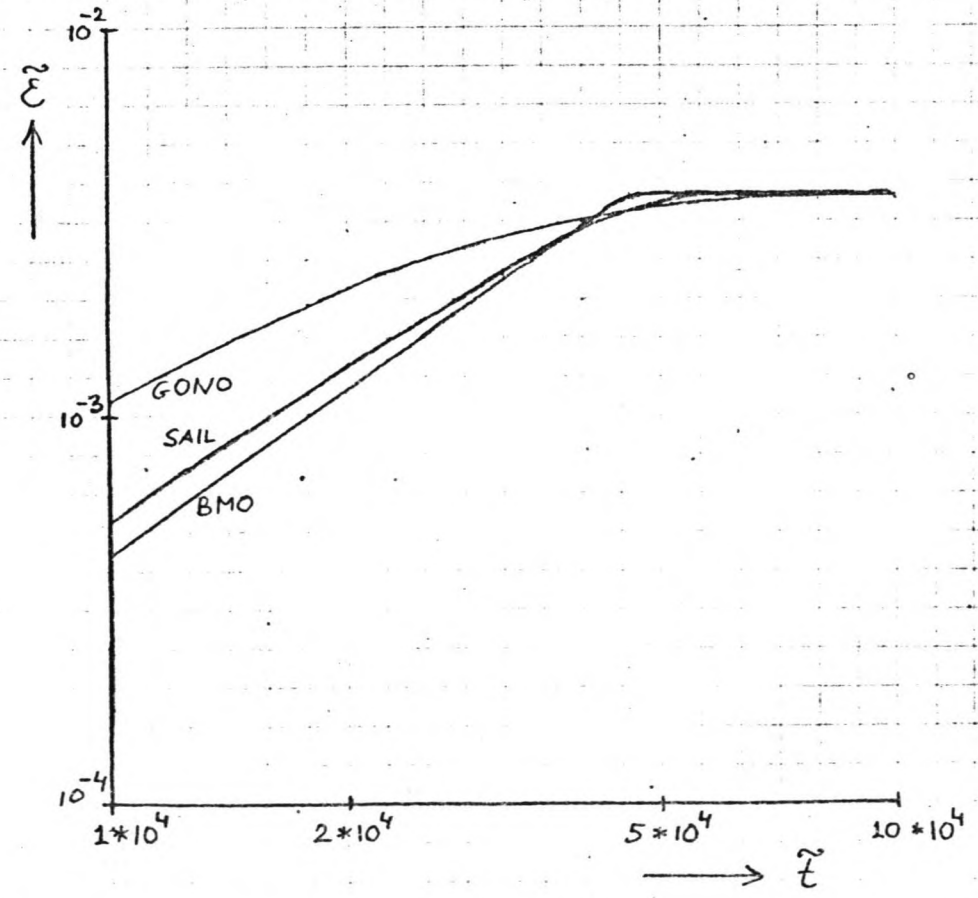


Fig. A.1 Plot of $\tilde{\varepsilon}$ vs. $\tilde{t}$ for three numerical wave prediction models.

Table A.1 Parameter values of three numerical wave prediction models and the chosen upper and lower limit

	a	b	c	d
SAIL	$3.6 * 10^{-3}$	$8.67 * 10^{-16}$	3.25	0.4
BMO	$3.6 * 10^{-3}$	$2.1 * 10^{-22}$	4.67	0.3
GONO	$3.6 * 10^{-3}$	$6.1 * 10^{-4}$	0.75	2.0
upper limit	$3.6 * 10^{-3}$	$1.9 * 10^{-20}$	4.67	0.3
lower limit	$2.4 * 10^{-3}$	$6.1 * 10^{-23}$	4.67	0.3

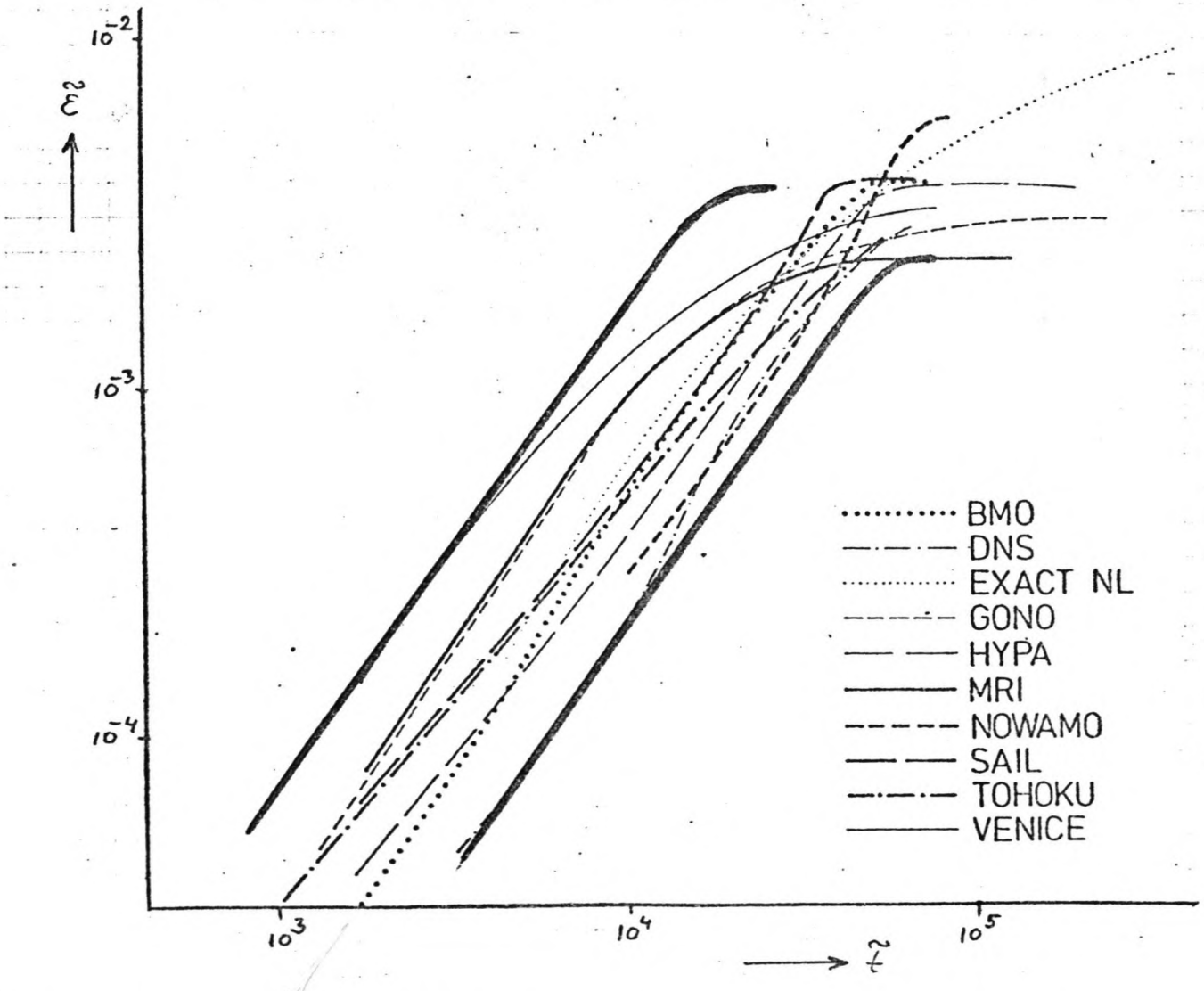


Fig. A.2 Family of wave growth curves presented in the SWAMP study with their upper and lower limit (thick lines).

Appendix B: Determination of the main wave direction

Nowadays several wave sensor systems exist which yield a possibility to estimate properties of directional wave spectra. Borgman (4) gives a survey of the mathematics involved. The familiar analysis to estimate the one-dimensional energy density spectrum, $E(f)$, is extended to estimate the two-dimensional energy density spectrum, $E(f,\theta)$. This two-dimensional spectrum can be written as the product of the frequency spectrum and a directional energy spreading function

$$E(f,\theta) = E(f)\, D_f(\theta) \qquad (B-1)$$

where

$$E(f) = \int_0^{2\pi} E(f,\theta)\, d\theta \qquad (B-2)$$

and

$$\int_0^{2\pi} D_f(\theta)\, d\theta = 1 \qquad (B-3)$$

Being continuous and periodic the directional spreading function can be expanded in an infinite Fourier series

$$D_f(\theta) = \frac{1}{\pi}\left\{\frac{1}{2} + \sum_{n=1}^{\infty}\left[a_n(f)\cos(n\theta) + b_n(f)\sin(n\theta)\right]\right\} \qquad (B-4)$$

with Fourier coefficients given by

$$a_n(f) = \int_0^{2\pi} D_f(\theta)\cos(n\theta)\, d\theta \qquad (B-5)$$

$$b_n(f) = \int_0^{2\pi} D_f(\theta)\sin(n\theta)\, d\theta \qquad (B-6)$$

The mean wave direction at frequency f is defined by

$$\theta_0(f) = \arctan\left(\frac{b_1(f)}{a_1(f)}\right) \qquad (B-7)$$

For the full frequency range, Fourier coefficients are defined by

$$a_n = \frac{\int_0^{\infty} a_n(f)\, E(f)\, df}{\int_0^{\infty} E(f)\, df} \qquad (B-8)$$

$$b_n = \frac{\int_0^{\infty} b_n(f)\, E(f)\, df}{\int_0^{\infty} E(f)\, df} \qquad (B-9)$$

Using these definitions the main wave direction is given by

$$\theta_o = \arctan\left(\frac{b_1}{a_1}\right) \qquad (B-10)$$

Appendix C: Relaxation models proposed in the literature

Günther et al. (8) propose a relaxation model for the direction of the total momentum flux, θ_0,

$$\frac{\partial \theta_0}{\partial t} = \chi \frac{U f_m^2}{g} \sin(\theta_w - \theta_0) \qquad (C-1)$$

in which χ is a nondimensional constant. From four suitable events occurring during the JONSWAP 73 experiment they derive an average value of

$$\chi = 2.1 * 10^{-3} \qquad (C-2)$$

Assuming that the main wave direction equals the direction of the total momentum flux, this model can be compared with the model derived in Chapter 2, thus yielding

$$\tilde{\tau} = \chi^{-1} \nu^{-2} \qquad (C-3)$$

where ν denotes the nondimensional peak frequency

$$\nu = \frac{U f_m}{g} \qquad (C-4)$$

The nondimensional peak frequency can be related to the nondimensional energy by using the result of Hasselmann et al. (11)

$$\tilde{\varepsilon} = K \nu^{-n} \qquad (C-5)$$

in which

$$K = 7.4 * 10^{-6} \qquad (C-6)$$

$$n = 3.05 \qquad (C-7)$$

Equation (C-3) can then be written as

$$\tilde{\tau} = \chi^{-1} \left(\frac{\tilde{\varepsilon}}{K} \right)^{2/n} \qquad (C-8)$$

A frequency dependent relaxation model for mean directions is proposed by Hasselmann et al. (9)

$$\frac{\partial \theta_0(f)}{\partial t} = 2\pi f b \sin(\theta_w - \theta_0(f)) \qquad (C-9)$$

with b depending on frequency and the ratio of wind velocity to wave celerity.

From the JONSWAP 73 experiment they derive an average value of

$$b = 2.0 * 10^{-5} \qquad (C-10)$$

Allender et al. (1) find an average value of

$$b = 1.7 * 10^{-5} \qquad (C-11)$$

One can assume the mean direction at the peak frequency to respond more or less the same as the mean direction of the full frequency range. The narrower the frequency spectrum the more true this will be. Using this assumption the frequency dependent model for $f = f_m$ can be compared with the model of Chapter 2, yielding

$$\tilde{\tau} = (2\pi \nu b)^{-1} \qquad (C-12)$$

With Equation (C-5) this becomes

$$\tilde{\tau} = (2\pi b)^{-1} \left(\frac{\tilde{\varepsilon}}{\kappa}\right)^{1/n} \qquad (C-13)$$

Appendix D: Directional response in Klatter's ECG model

Klatter (18) considers the directional response behaviour of his ECG wave prediction model by investigating a case with a stationarily turning wind.
The wind direction turns with a constant angular velocity, Ω. After reaching an equilibrium, the wave direction will be turning with the same angular velocity, but lagging behind the wind direction. The lag angle, φ, remains constant

$$\varphi = \Omega T \qquad (D-1)$$

with T denoting the lag time.
Here Equation (2-15) yields

$$\tilde{\tau} = \frac{g}{U} \frac{\sin \varphi}{\Omega} \qquad (D-2)$$

Klatter's results and computed values of $\tilde{\tau}$ are listed below.

Table D. 1 Results from Klatter's ECG wave prediction model

U [m/s]	Ω [deg/hour]	$\tilde{\varepsilon} * 10^3$ [-]	φ [deg]	$\tilde{\tau} * 10^{-3}$ [-]
20	5	1.98	56	16.8
20	10	1.05	64	9.1

Appendix E: Correction for the difference angle

Assume $\theta_o = \theta_w$ and the directional energy spreading function to be given by

$$D_f(\theta) = \frac{2}{\pi}\cos^2(\theta-\theta_o) \quad \text{for } |\theta-\theta_o| < \frac{\pi}{2} \tag{E-1}$$

$$D_f(\theta) = 0 \quad \text{for } |\theta-\theta_o| \geq \frac{\pi}{2} \tag{E-2}$$

Integration over direction yields

$$\int_{-\pi}^{\pi} D_f(\theta)\, d\theta = 1 \tag{E-3}$$

After a change in wind direction, Δ, only a part of the extant energy will contribute to the new directional spreading function. This is represented by the shaded area in Figure E.1, which is given by

$$2\int_{\theta_o+\frac{\Delta}{2}}^{\theta_o+\frac{\pi}{2}} \frac{2}{\pi}\cos^2(\theta-\theta_o)\, d\theta = \frac{\pi-\Delta-\sin\Delta}{\pi} \tag{E-4}$$

Therefore the correction for the difference angle, Δ, consists of introducing a lower energy level, $\tilde{\mathcal{E}}^*$, given by

$$\tilde{\mathcal{E}}^* = \frac{\pi-\Delta-\sin\Delta}{\pi}\,\tilde{\mathcal{E}} \tag{E-5}$$

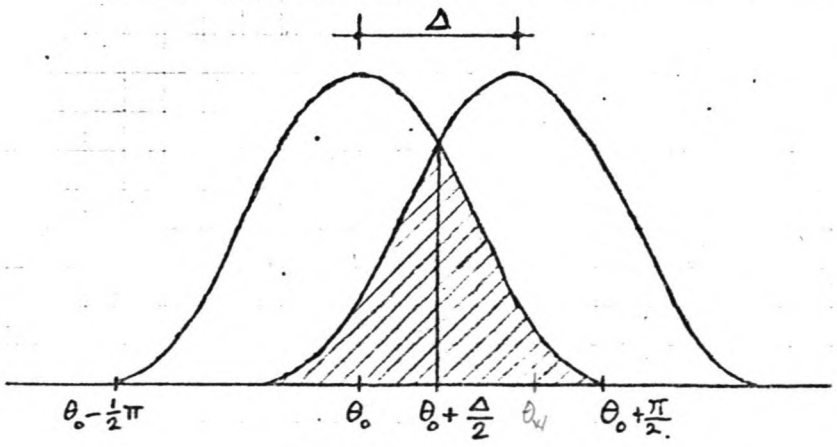


Fig. E.1 Graph to illustrate the correction for the difference angle.